The 2014 World Congress on
Advances in Civil, Environmental, and Materials Research (ACEM14)
Busan, Korea, August 24-28, 2014

Effect of Co Doping on Structural Properties of Hematite Thin Films

*Aseya Akbar[1)] Saira Riaz[2)], Zohra N Kayani[3)] and Shahzad Naseem[2)]

[1), 2)] Centre of Excellence in Solid State Physics, University of the Punjab, Lahore 54590, Pakistan
[3)] Department of Physics, LCWU, Lahore, Pakistan
* saira.cssp@pu.edu.pk

ABSTRACT

Amongst various phases of iron oxide, hematite (α-Fe_2O_3) is the most stable and has found wide applications in spintronic and data storage devices and as a catalyst. Undoped and doped thin films are prepared by sol-gel and spin coating method. Films are characterized structurally using Bruker D8 Advance X-ray diffractometer. The presence of diffraction peaks corresponding to to (012), (104), (110), (006), (113), (202), (024), (214) and (217) confirms the formation of pure hematite phase at 300^{o}C. XRD results indicate that peak positions shift to higher angles due to the difference in ionic radius of cobalt and iron. Crystallite size increases from 28nm to 38nm with increase in dopant concentration to 5%. Increase in dopant concentration to 7% results in decrease in crystallite size indicating the possibility that some of the dopant atoms occupy the interstitial sites or are sitting on the grain boundaries thus resulting in decrease in crystallite size. In addition, the strain induced in films as the result of high dopant concentration also leads to reduction in crystallite size. Dislocation density calculated using XRD results indicate that number of dislocation lines increases as the dopant concentration is increased from 7-9% resulting in destruction of crystalline structure. Increase in x-ray density (5.0-5.1g/cm^3) and reduction in porosity (0.12-0.100%) of the films indicates increased packing density of the films with replacement of cobalt with iron.

1. INTRODUCTION

Functional metal oxides have been of interest in scientific community in the last decade due to their unique properties. Among these, iron oxide is of particular interest due to their catalytic, spintronic and biomedical applications (Riaz 2014(a,b), Lian 2012, Akbar 2014(a)). Iron oxide exists in three forms i.e. FeO, Fe_2O_3 and Fe_3O_4 (Riaz 2013). Fe_2O_3 is further categorized as α-Fe_2O_3, γ-Fe_2O_3, ε-Fe_2O_3 and β-Fe_2O_3. α-Fe_2O_3 is the most stable form of iron oxide (Garcia 2013, Glasscock 2008).

Hematite (α-Fe_2O_3) crystallizes in rhombohedral structure belonging to R3c space

[2] Professor
[1)] Graduate Student

group or in hexagonal system with D_{3d}^6 (Yogi 2013, Zachary 2011, Rivera 2012). In orthorhombic system, the lattice parameters of α-Fe_2O_3 are a=5.427Å and α=55.3˚. In hexagonal system the lattice parameters of α-Fe_2O_3 are a=5.034Å and c=13.75Å. Oxygen anions are arranged in hexagonal close pack arrangement. 2/3 of the octahedral sites are occupied by Fe^{3+} cations. The structure is composed of layers of oxygen and iron normal to three-fold axes. (Yogi 2013)

Magnetic properties of α-Fe_2O_3 are of considerable attention. It is antiferromagnetic with Neel temperature of 950K. In the temperature range of 950-260 K rhombohedral (111) planes are arranged in the form layers of Fe^{3+} cations (Zachary 2011). Oxygen anions separate consecutive planes. Ferromagnetic coupling arises between the spins in (111) plane below 300K. Antiferromagnetic coupling arises between the adjacent planes. This results in spin canting between (111) planes. Due to this, uncompensated Fe^{3+} spins are present between the two neighboring planes (Yogi 2013). This induces weak or canted ferromagnetic behavior in antiferromagnetic α-Fe_2O_3. Below 260K, direction of spin changes. This temperature of 260K is known as Morin temperature. The spins are completely perpendicular to (111) plane. This results in antiferromagnetic behavior of α-Fe_2O_3 (Yogi 2013, Akbar 2014(b))

In order to enhance the properties of α-Fe_2O_3, we here report the structural properties of cobalt doped hematite thin films using sol-gel method. The dopant concentration is varied as 1%, 3%, 5%, 7% and 9%. The films are annealed at 300˚C for 60mins. Changes in structural properties are correlated with variation in dopant concentration.

2. EXPERIMENTAL DETAILS

Cobalt doped iron oxide sols were prepared using sol-gel method. $Fe(NO_3)_3.9H_2O$ was dissolved in deionized (DI) water. The solution was stirred at room temperature. Ethylene glycol was added to the above solution. The solution was then heated on hot plate at 60˚C. Details of sol-gel synthesis are reported earlier (Akbar 2014(b)). For cobalt doping, cobalt nitrate was dissolved in DI water and added to iron oxide sol. the dopant concentration was varied as 1-9%. The sol was spin coated on copper substrate. Before spin coating, copper was firstly etched using diluted HCl and the then rinsed repeatedly in DI water. The substrates were then place in ultrasonic vibrator in acetone and isopropyl alcohol for 10 and 15mins, respectively (Asghar 2006(a), (b)). After spin coating the films were annealed at 300˚C for 60mins.

Films were characterized structurally using Bruker D8 Advance X-ray Diffractometer with Cukα=1.5406Å.

2. EXPERIMENTAL DETAILS

Fig. 1 show XRD patterns for undoped and cobalt doped iron oxide thin films. Presence of diffraction peaks corresponding to (012), (104), (110), (006), (113), (202), (024), (214) and (217) indicate the formation of α-Fe_2O_3 phase of iron oxide. No peaks corresponding to aluminum and/or aluminum oxide were observed even at dopant concentration of 9% (Fig. 1(c)). Slight shift of peaks positions is observed with increase in dopant concentration due to slight difference in ionic radius of cobalt as compared to

iron. The shift in peak positions indicates that the dopant has been successfully incorporated in the host lattice.

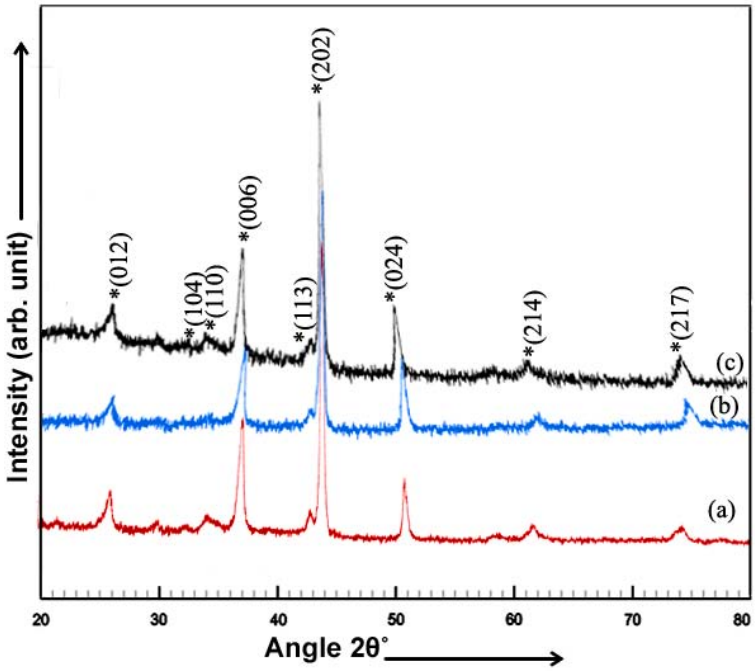

Fig. 1 XRD patterns for cobalt doped iron oxide thin films with dopant concentration (a) 1% (b) 5% (c) 9%

Crystallite size (*t*), strain (*Δd/d*) and dislocation density (*δ*) (Cullity 1956) of aluminum doped iron oxide thin films is calculated using Eq. (1)-(4)

$$t = \frac{0.9\lambda}{B\cos\theta} \tag{1}$$

$$Strain = \frac{\Delta d}{d} = \frac{d_{\exp} - d_{pdf}}{d_{pdf}} \tag{2}$$

$$\delta = \frac{1}{t^2} \tag{3}$$

Where, *λ* is the wavelength (1.5406Å), *B* is the full width at half maximum, d_{exp} is the d-spacing calculated from XRD pattern and d_{pdf} is the d-spacing taken from JCPDS card no. 87-1165, *θ* is the diffraction angle.

Crystallite size and crystallinity of cobalt doped iron oxide thin films are plotted as a function of dopant concentration in Fig. 2(a). Crystallite size increases from 28.8nm to 37.9nm as the dopant concentration is increased to 5%. With further increase in dopant concentration, crystallite size decreased to 27nm. It can be predicted that at low dopant concentration the atoms occupy the substitutional positions. At high dopant concentration, the probability of dopant atoms residing on grain boundaries increases (Akbar 2014(b)). This leads to destruction in crystallite size. In addition, strain in thin films also affects the crystallite size (Riaz 2007). Decrease in strain with increase in dopant concentration to 5% (Fig. 2(b)) also resulted in increase in crystallite size. The

increased crystallite size thus resulted in few number of grain boundaries. The reduced number of grain boundaries at low dopant concentration thus resulted in decreased dislocations in thin films (Fig. 2(b)).

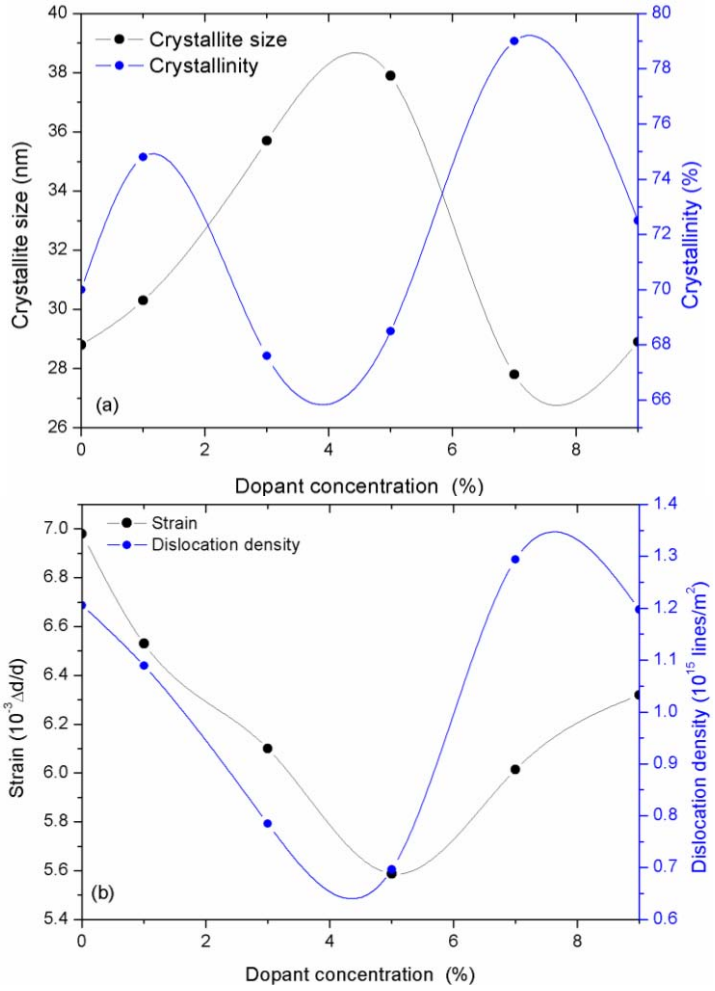

Fig. 2 (a) Crystallite size and crystallinity (b) strain and dislocation density plotted as a function of dopant concentration for Co doped iron oxide thin films

Lattice parameters (*a,c*), x-ray density (ρ) and porosity of aluminum doped Fe_2O_3 thin films is calculated using Eq. (4)-(6).

$$\sin^2\theta = \frac{\lambda^2}{3a^2}\left(h^2 + k^2 + hk\right) + \frac{\lambda^2 l^2}{4c^2} \tag{4}$$

$$\rho = \frac{1.66042\,\Sigma A}{V} \tag{5}$$

$$Porosity(\%) = \left[1 - \frac{\rho_{\exp}}{\rho_{std}}\right] \times 100 \tag{6}$$

Where, *(hkl)* represent the miller indices, ΣA is the sum of atomic weights of the atoms in the unit cell, V is the volume of unit cell (V=0.866a^2c), ρ_{exp} is the experimental density calculated using Eq. (5), ρ_{std} is bulk density of iron oxide.

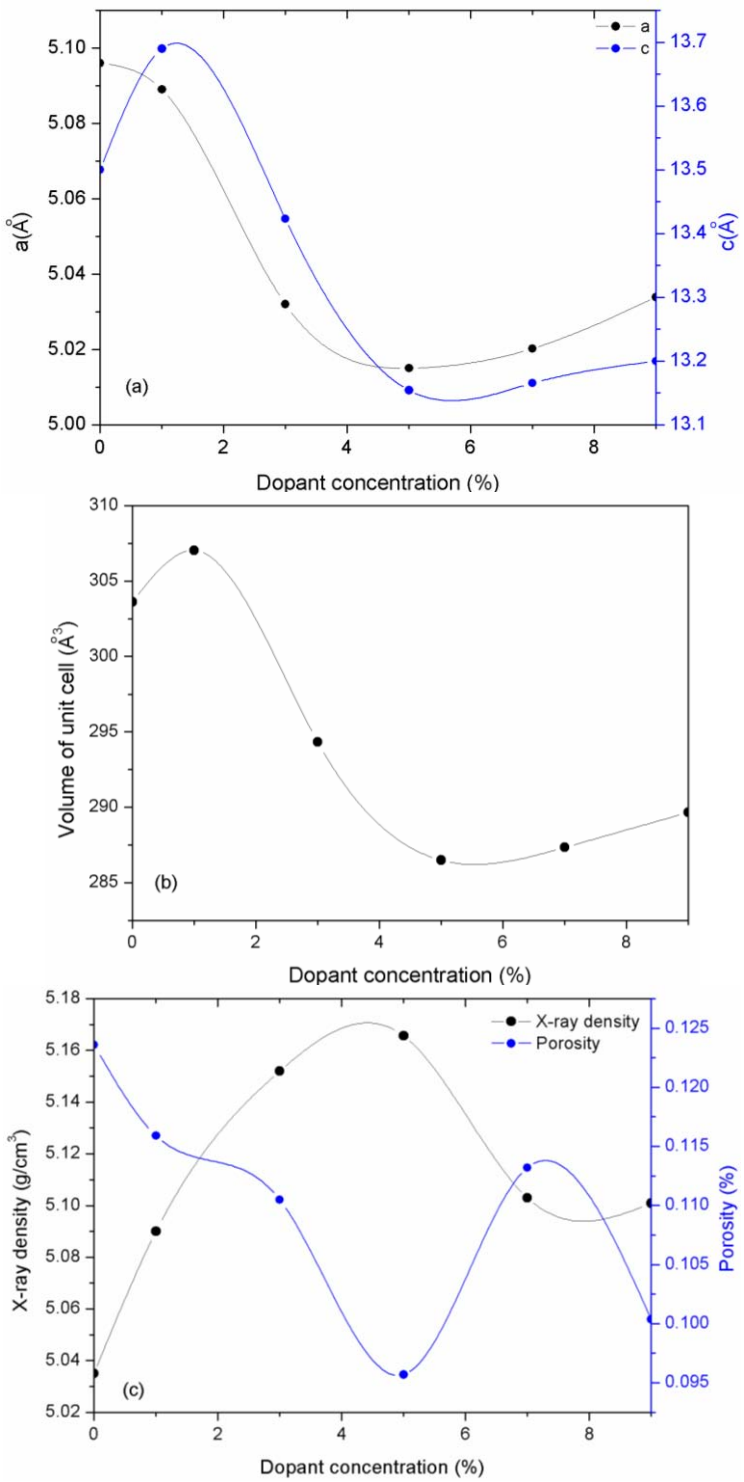

Fig. 3 (a) Lattice parameters (b) volume of unit cell (c) x-ray density and porosity of cobalt doped iron oxide thin films plotted as a function of dopant concentration

Fig. 3(a) show lattice parameters plotted as a function of dopant concentration. The lattice parameters decreased as the dopant concentration was increased to 5% thus leading to reduction in unit cell volume. This decrease in unit cell volume from 303Å to 286Å is due to smaller ionic radius of cobalt as compared to that of iron. This reduced unit cell volume leads to increased density of the films (Fig. 3(b)) indicating more compact structure of cobalt doped iron oxide thin films.

Although no peaks corresponding to aluminum or aluminum oxide were observed in XRD pattern (Fig. 1) even with high dopant concentration of 9% but variation in crystallite size (Fig. 2(a)) and lattice parameters (Fig. 3(b)) strongly indicated that the dopant has been successfully incorporated in the α-Fe_2O_3 lattice.

3. CONCLUSIONS

Cobalt doped iron oxide thin films were prepared using sol-gel and spin coating method. The dopant concentration is varied as 1-9%. No peaks corresponding to dopant atom or its oxide were observed even at high dopant concentrations. The crystallite size decreased from 28.8nm to 38nm with increase in dopant concentration to 5%. Further increasing the dopant concentration resulted in decreased crystallite size and increased dislocation density. Variation in lattice parameters and unit cell volume strongly indicate the incorporation of dopant atoms on the substitutional sites in α-Fe_2O_3 lattice.

REFERENCES

Akbar, A., Riaz, S., Bashir, M. and Naseem, S. (2014(a)), "Effect of Fe^{3+}/Fe^{2+} ratio on superparamagnetic behaviour of spin coated iron oxide thin films," *IEEE Trans. Magn.*, doi: 10.1109/TMAG.2014.2312972.

Akbar, A., Riaz, S., Ashraf, R. and Naseem, S. (2014 (b)), "Magnetic and magnetization properties of Co-doped Fe_2O_3 thin films," *IEEE Trans. Magn.*, doi: 10.1109/TMAG.2014.2311826

Asghar, M.H., Placido, F. and Naseem, S. (2006(a)), "Characterization of reactively evaporated TiO_2 thin films as high and medium index layers for optical applications," *Eur. Phys. J. - Appl. Phys.*, **35**, 177-184.

Asghar, M.H., Placido, F. and Naseem, S. (2006(b)), "Characterization of Ta_2O_5 thin films prepared by reactive evaporation," *Eur. Phys. J. - Appl. Phys.*, **36**, 119-124.

Cullity, B.D. (1956), "Elements of x-ray diffraction," Addison Wesley Publishing Company, USA.

Garcia, H.A., Melo Jr., R.P., Azevedo, A. and Araujo, C.B. (2013), "Optical and structural characterization of iron oxide and cobalt oxide thin films at 800 nm," *Appl. Phys. B.*, **111**, 313-321

Glasscock, J.A., Barnes, P.R.F., Plumb, I.C., Bendavid, A. and Martin, P.J. (2008), "Structural, optical and electrical properties of undoped polycrystalline hematite thin films produced using filtered arc deposition," *Thin Solid Films*, **516**, 1716-1724.

Lian, X., Yang, X., Liu, S., Xu, Y., Jiang, C., Chen, J. and Wang, R. (2012), "Enhanced photoelectrochemical performance of Ti-doped hematite thin films prepared by the sol–gel method," *Appl. Surf. Sci.*, **258**, 2307– 2311

Riaz, S. and Naseem, S. (2007), "Effect of reaction temperature and time on the structural properties of Cu(In,Ga)Se_2 thin films deposited by sequential elemental layer technique," *J. Mater. Sci. Technol.*, **23**, 499-503

Riaz, S., Akbar, A. and Naseem, S. (2013), "structural, electrical and magnetic properties of iron oxide thin films," *Adv. Sci. Lett.*, **19**, 828-833.

Riaz, S., Akbar, A. and Naseem, S. (2014(a)), "Controlled nanostructuring of multiphase core-shell iron oxide nanoparticles," *IEEE Trans. Magn.*, **50**, 2300204

Riaz, S., Bashir, M. and Naseem, S. (2014(b)), "Iron Oxide Nanoparticles Prepared by Modified Co-Precipitation Method," *IEEE Trans. Magn.*, **50**, 4003304

Rivera, R., Pinto, H.P., Stashans, A. and Piedra, L. (2012), "Density functional theory study of Al-doped hematite," *Phys. Scr.*, 85, 015602

Suresh, R., Prabu, R., Vijayaraj, A., Giribabu, K., Stephen, A. and Narayanan, V. (2012), "Facile synthesis of cobalt doped hematite nanospheres: Magnetic and their electrochemical sensing properties," *Mater. Chem. Phys.*, **134**, 590-596

Valdes, A.H., Zarate, R.A., Martinez, A.I., Canul, M.I.P., Lobato, M.A.G. and Villaroel, R. (2014), "The role of solvents on the physical properties of sprayed iron oxide films," *Vacuum*, **105,** 26-32

Varshney, D. andYogi, A. (2013), "Influence of Cr and Mn substitution on the structural and spectroscopic properties of doped hematite: α-$Fe_{2-x}M_xO_3$ ($0.0 \leq x \leq 0.50$)," *J. Molecular Structure*, **1052**, 105–111

Yogi, A. and Varshney, D. (2013), "Magnetic and structural properties of pure and Cr-doped hematite: α-$Fe_{2-x}Cr_xO_3$ ($0 \leq x \leq 1$)," *J. Adv. Ceram.*, **2**, 360-369

Zachary, D., Pozun and Henkelman, G., "Hybrid density functional theory band structure engineering in hematite," *J. Chem. Phys.*, **134**, 224706